PHYSICAL REVIEW B VOLUME 60, NUMBER 24 15 DECEMBER 1999-II

Percolation problem in atomic transport in $Hg_{1-x}Cd_xTe$

N. Mainzer
Department of Materials Engineering, Technion-Israel Institute of Technology, Haifa 32000, Israel and SCD-Semiconductor Devices, P.O. Box 2250/99, Haifa 31021, Israel

E. Zolotoyabko
Department of Materials Engineering, Technion-Israel Institute of Technology, Haifa 32000, Israel and Solid State Institute, Technion-Israel Institute of Technology, Haifa 32000, Israel

(Received 22 June 1999)

Using high-resolution x-ray diffraction for precise measurements of structural modifications in boron-implanted $Hg_{1-x}Cd_xTe$ layers, we found a percolation problem in the long-range diffusion of Cd interstitials through the Cd, Hg sublattice. The percolation threshold $x_c = 0.265$ is in agreement with the calculated one, $x_{th} = 0.278$, for dumbbell interstitials diffusion in the fcc lattice [J. Bocquet, Phys. Rev. B **50**, 16 386 (1994)]. These findings were supported by high-resolution scanning electron microscopy images, taken under magnification ×400 000, in which very different post-implantation surface recovery (due to a flux of interstitials from an interior to the crystal surface) was observed below and above $x = x_c$. Measurements of x-ray-diffraction profiles in samples, implanted and annealed at 150–350 °C, allowed us to determine an energy barrier, $\Delta E = 0.31$ eV, between Cd-Cd and Cd-Hg dumbbell configurations. [S0163-1829(99)10547-2]

I. INTRODUCTION

Recently, Cahen *et al.*[1,2] pointed out a percolation problem in the Ag-doped semiconductor $Hg_{1-x}Cd_xTe$ with $x \approx 0.8$ (Cd-rich region of the composition scale). They found drastic changes in the Ag diffusion coefficient and doping properties, as a function of Cd-content, x. Above $x \approx 0.8$ (i.e., when the Hg content is less than $1 - x \approx 0.2$), the Ag doping results in the material being n-type, and the room-temperature Ag-diffusion coefficient being low, $D < 10^{-15}$ cm^2/sec. Just below $x \approx 0.8$, the diffusion coefficient rises up to $D > 10^{-8}$ cm^2/sec, and this is accompanied by material transformation to p-type. These findings are explained in terms of Ag percolation via Hg sites. Taking account of percolation phenomena leads indeed to completely different rates of atomic transport below and above a percolation threshold, x_{th}. The latter equals theoretically $1 - x_{th} = 0.19$ for atomic jumps via fcc sites (see, e.g., Ref. 3).

In this paper we introduce more conventional $Hg_{1-x}Cd_xTe$ structures with $x \approx 0.2$–0.3 (Hg-rich region of the compositional scale) into a percolation domain. These semiconductor alloys are widely used in infrared detector technology,[4–6] e.g., for detection of photons having a wavelength in a range of 8–14 or 3–5 μm (atmospheric transparency windows).

A common way to form n-p junctions in $Hg_{1-x}Cd_xTe$-based photovoltaic devices is boron implantation.[7–10] Contrary to IV-group or III–V-group semiconductors, the conductivity of the B-implanted $Hg_{1-x}Cd_xTe$ is not directly determined by the B doping but rather by the implantation damage. The latter results in the n-type conductivity and is used to fabricate the n^+ layer on the initially p-type $Hg_{1-x}Cd_xTe$ for detector functioning.[11–14] So, the study of defect formation and subsequent diffusion processes in implanted $Hg_{1-x}Cd_xTe$ is of great importance to electrical properties.

However, there is a lot of controversy between different groups concerning an identification of electrically active types of defects, as well as regarding the role of boron activation in the creation of n-p junction.[4,8,10,11,15–19] For example, several groups[8,11,17–19] reported that the n-type conductivity is caused by lattice damage induced by B implantation into the p-type $Hg_{1-x}Cd_xTe$, but expressed contradictory opinions of boron activation. Some authors[8,19] did not succeed in boron activation, in contrast with other groups[11,17,18] that claimed partial or full success. Transmission electron microscopy studies[10,16] diverge in their conclusions regarding what type of point defects, interstitials or vacancies, prevails in the damaged layer. A similar controversy exists among x-ray results. In Ref. 20, an additional peak in the x-ray-diffraction profiles has been found after B implantation, which could be attributed to the lattice swelling due to excess of interstitials in the damaged layer. On the contrary, Ref. 21 is concentrated on the vacancy-related features in the x-ray-diffraction profiles. A deeper look at all mentioned results indicates that the controversy mentioned could be driven by small differences in Cd content, x, of implanted samples.

This paper focuses on the structural modifications induced by boron implantation in $Hg_{1-x}Cd_xTe$ layers with different Cd content, x. The creation of point defects and their dynamics were investigated by high-resolution x-ray diffraction (HRXRD) and high-resolution scanning electron microscopy (HRSEM).

II. EXPERIMENT

A. Sample preparation

Four different sets of samples were used in the present study, viz., samples grown by liquid phase epitaxy (LPE), by metalorganic chemical vapor deposition (MOCVD), by molecular-beam epitaxy (MBE), and by the Bridgman bulk

0163-1829/99/60(24)/16715(7)/$15.00 PRB 60 ©1999 The American Physical Society

growth method. The LPE layers of $Hg_{1-x}Cd_xTe$ (20 μm thick, $0.19<x<0.67$) were grown on (111)B CdZnTe substrates. The annealed, undoped layers of this kind revealed p-type conductivity due to Hg vacancies. The MOCVD layers of $Hg_{1-x}Cd_xTe$ (15 μm thick, $0.22<x<0.37$) were grown on (211)B CdTe substrates and covered with the 90–110-nm-thick CdTe capping layer. The MBE samples were also grown on (211)B-oriented CdZnTe substrates. The thicknesses of the $Hg_{1-x}Cd_xTe$ and the CdTe cap layers, composing $CdTe/Hg_{1-x}Cd_xTe$ $(0.24<x<0.35)$ heterostructures, were 10 μm and 80 nm, respectively. The Bridgman-grown sample was a 600-μm-thick (111)-oriented CdTe slice (i.e., with $x=1$).

The electrical characteristics of the samples were measured by the van der Pauw–Hall method at 77 K in a magnetic field of 0.1 T, and the Cd content was measured by Fourier-transform infrared transmission (FTIR), which, as was shown in Ref. 22, provides rather accurate data with an absolute precision of $\delta x \leqslant 0.01$.

All samples were implanted with B^+ ions at room temperature with a dose of 1×10^{15} ions/cm^2 and an energy of 250 keV. The penetration depth of B^+ ions into $Hg_{1-x}Cd_xTe$ is $R_p \approx 500$ nm and the straggling parameter is around 150 nm. Part of the implanted samples were subjected to heat treatments in a forming gas environment for 1 h at temperatures 150–350 °C. Structural modifications in implanted and annealed samples were examined by HRXRD and surface quality was examined by HRSEM.

B. Experimental techniques

HRXRD measurements were carried out with a Bede D^3 x-ray diffractometer combined with an 18 kW Rigaku rotating anode generator. A highly monochromatized Cu $_{K\alpha_1}$ line was chosen from the primary x-ray beam by means of two channel-cut (220) Si crystals, which produced a $0.1\times10\,\mathrm{mm}^2$ spot on the sample surface. The (333) or (422) diffraction profiles, depending of the substrate orientation, were taken using a triple-axis mode of measurement. In this mode the diffracted beam, before entering the detector, passes through the (220)Si channel-cut crystal analyzer, which provided high resolution of the detecting system and, correspondingly, the high precision to the implantation-induced modifications of the lattice parameter, $\Delta a/a$. The setup allowed us to perform the relative lattice parameter measurements with an accuracy of $\Delta a/a \approx 10^{-5}$.

HRSEM images (plain views) of the samples were taken by means of LEO Gemini 982 FEG-SEM working at electron beam energies between 1 and 4 keV and magnifications up to $\times$400 000 with an aperture of 2–3 mm.

III. EXPERIMENTAL RESULTS AND DISCUSSION

Nowadays, HRXRD is a well-established technique for the measurements of lattice parameters with depth resolution,[23] which indeed is very suitable for implantation problems. By comparing the experimental HRXRD profile, measured in close vicinity to the Bragg angle, Θ_B, to the simulated one (using dynamical diffraction theory), one can derive modifications of lattice parameters as a function of crystal depth (see, e.g., Ref. 24). If the x-ray penetration length, L_x, is larger than the ion stopping length, R_p, and the implantation damage is rather high (this is exactly our case), diffraction signals from the damaged layer and undamaged region (crystal bulk) are well separated in an angular scale (see Fig. 1). The separation, $\Delta\Theta$, is proportional to the changes, $\Delta d/d$, of the interplanar spacing in the damaged layer, $(d+\Delta d)$, relative to that of the crystal bulk, d:

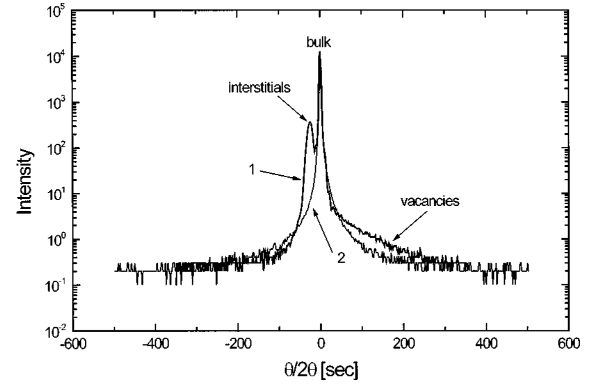

FIG. 1. Typical HRXRD profile (1) taken from an as-implanted $Hg_{1-x}Cd_xTe$ layer. HRXRD profile (2) taken from a virgin layer (before implantation) is shown for comparison.

$$\Delta\Theta = -\tan\Theta_B \frac{\Delta d}{d}. \tag{1}$$

So, using Eq. (1), it is possible to obtain valuable structural information on the damaged layers even without dynamical diffraction simulations. In some cases, post-implantation point defects of different type (for instance, vacancy and interstitials) are spatially separated due to the difference in migration rates, and the damaged layer is composed of sublayers which are enriched by defects of a certain type. In $Hg_{1-x}Cd_xTe$ structure, the interstitial atoms cause lattice swelling $(\Delta d/d>0)$, while vacancies cause lattice contraction $(\Delta d/d<0)$.[25] Correspondingly, coherent scattering, originating in crystalline layers with an average lattice parameter being larger or smaller than that of the bulk crystal, will produce additional diffraction features located [according to Eq. (1)] to the left side of the bulk peak (for the interstitials-rich layer) and to the right side of the bulk peak (for the vacancy-rich layer). These features are clearly seen in the typical HRXRD profile taken from an as-implanted (250 keV B^+ ions, dosage 1×10^{15} ions/cm^2) LPE-grown $Hg_{1-x}Cd_xTe$ sample $(x=0.25)$ and shown in Fig. 1. The interstitials-induced feature appears as a rather sharp diffraction peak because the interstitials-rich sublayer is well-confined around the depth R_p, where most of the lattice defects are created. In fact, according to dynamic diffraction fittings of HRXRD profiles measured in implanted crystals (see, e.g., Refs. 24 and 26), a sharp jump in $(\Delta d/d)$ appears (independently of the implanted ion and the matrix types) at the end of the ion trajectories (at a depth R_p), where ion velocities are close to zero and they cause maximum damage. It is reasonable to assume that the change of lattice parameter in the sublayer, confined at a depth R_p, is proportional to the interstitials concentration, C. Thus, the measurement of the angular separation, $\Delta\Theta$, between interstitials-

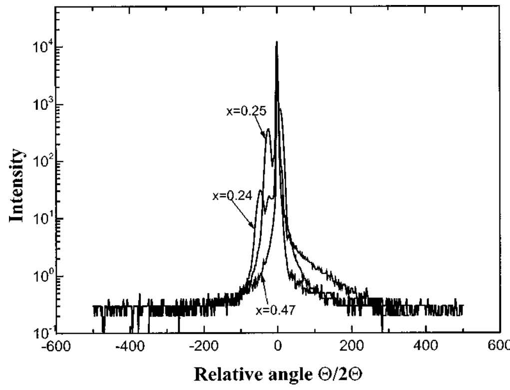

FIG. 2. HRXRD profiles taken from the LPE-grown layers with $x=0.24$, 0.25, and 0.47, subjected to B implantation.

induced and bulk peaks, according to Eq. (1), can be directly used as a measure of the C value.

This approach was used throughout the research in order to follow interstitials creation and post-implantation migration of point defects in differently grown and treated $Hg_{1-x}Cd_xTe$ layers. Selected HRXRD profiles, taken from the LPE-grown samples with different Cd content, x, are shown in Fig. 2. It is seen that the $\Delta\Theta$ value, in fact, strongly depends on x. The angular separation decreases if x is changing from $x=0.24$ to 0.25. In the sample with $x=0.47$, the interstitials peak is completely missing. A very similar behavior was observed in the MOCVD and MBE samples. The measured $\Delta d/d$ values for all samples involved in this research are plotted in Fig. 3 versus Cd content, x. The function $\Delta d/d(x)$ [and related interstitials concentration, $C(x)$] exhibits remarkable steplike shape with a very sharp drop confined within $0.25<x<0.28$. Interstitials concentration, $C(x)=k(\Delta d/d)(x)$, inside an implanted layer [which is proportional to the measured swelling of the lattice parameter, $(\Delta d/d)(x)$], can be fitted well by a function

$$C(x)=\frac{A}{1+\exp[(x-x_c)/\varepsilon]},\qquad A=C(0)\left[1+\exp\left(-\frac{x_c}{\varepsilon}\right)\right], \tag{2}$$

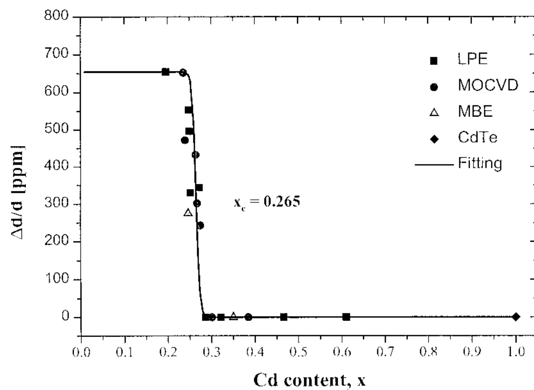

FIG. 3. Measured $(\Delta d/d)$ values in implanted $Hg_{1-x}Cd_xTe$ layers grown by different techniques: squares LPE; circles, MOCVD; triangles, MBE, as a function of Cd content, x. Diamond symbol relates to CdTe. Solid line represents fitting of experimental data by Eq. (2).

where x_c is the critical concentration, which defines the step position in the x scale, and ε is the fitting parameter, defining the step width. If $\varepsilon \ll 1$ (and this is the case), $C(0)\approx A$. The best fit of the experimental data, shown in Fig. 3, by function (2) occurs at $x_c=0.265$ and $\varepsilon=0.004$. Steplike behavior of $C(x)$ unambiguously points out a percolation problem[27] in the migration of point defects created by implantation.

In fact, TRIM (transport of ions in matter) simulations of lattice damage induced by B implantation in $Hg_{1-x}Cd_xTe$ layers with different x values showed that the amounts of displaced atoms of a certain type, Hg, Cd, or Te, are proportional to atomic concentrations inside the layer. An experimental study[28] of the implantation damage in $Hg_{1-x}Cd_xTe$ by channeling Rutherford backscattering spectroscopy also demonstrated only a gradual damage buildup, as a function of x. So, there is no reason for sharp changes in the $C(x)$ dependence at the stage of defect production. It means that understanding of experimental findings, shown in Fig. 3, should take into account post-implantation defect transport. At this stage a percolation problem could be of great importance, since the diffusion coefficient is very sensitive to the compositional changes in close vicinity to the percolation threshold, x_c.

Before discussing an atomic model for percolation in the $Hg_{1-x}Cd_xTe$ layers, let us correlate defect concentrations, $C(x)$, remaining frozen within the implanted layer, with an x-dependent diffusion coefficient, $D(x)$.

We consider, in the first approximation, that most of the lattice defects with concentration $C(L,t=0)$ are produced at time moment $t=0$ at a depth L. This nonequilibrium state tends to disappear with time, and atomic migration as well as defect recombination are the driving forces for smearing of concentration peculiarity. Let us assume that the $C(L,t)$ function obeys the diffusion equation:

$$\frac{dC(L,t)}{dt}=-D(x)\frac{\partial^2 C(L,t)}{\partial z^2}. \tag{3}$$

However, in our case it is not so easy to find an exact analytic solution because of the important role of defect recombination processes.[26] Setting $C=0$ at the crystal surface (infinite sink), the right-side term in Eq. (3) can be roughly estimated as $C(L,t)/L^2$, which yields

$$\frac{dC(L,t)}{dt}=-D(x)\frac{C(L,t)}{L^2}. \tag{4}$$

This approximation can be used near the maximum of the Gaussian-like defect distribution, where $\exp(-z^2/2\sigma^2)\approx 1-z^2/2\sigma^2$, and if $\sigma\approx L$. Equation (4) can be easily integrated, providing

$$C(L,t)=C(L,0)\exp\left(-\frac{D(x)t}{L^2}\right). \tag{5}$$

Equation (5) describes general exponential relaxation of a system being not far from equilibrium conditions.[29] It yields an important relationship between diffusion coefficient and defect concentration measurable by HRXRD:

$$D(x)=\frac{L^2}{t_0}\ln\frac{C(L,0)}{C(L,t_0)}=\frac{L^2}{t_0}\ln\frac{C(0)}{C(x)}. \tag{6}$$

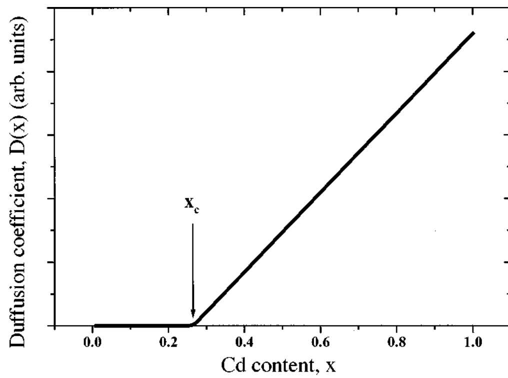

FIG. 4. Concentration-dependent diffusion coefficient, $D(x)$, for Cd interstitials in $Hg_{1-x}Cd_xTe$, indicating a percolation problem at $x<x_c$.

In Eq. (6) the $C(L,t_0)$ value is the defect concentration, remaining in the sample after a diffusion period t_0. Thus, $C(L,t_0)\equiv C(x)$, and is measured by HRXRD. As the $C(L,0)$ value we can take the concentration of interstitials in samples with Cd content well below the percolation threshold, i.e., when all of the interstitials appearing during implantation remain to be frozen, i.e., $C(x=0)\equiv C(0)$. Now, the diffusion coefficient $D(x)$ can be derived from experimental data by using the fitting function (2). A result of this procedure is plotted in Fig. 4, indicating that the $D(x)$ behavior greatly differs above and below the percolation threshold x_c

In fact, according to Eq. (2), $C(x)\approx C(0)$ at $x-x_c \ll \varepsilon$, which after substituting into Eq. (6) yields $D(x)\approx 0$. So, at $x<x_c$, the defect movements are confined inside small isolated clusters and there is no long-range defect diffusion to the sample surface [see Fig. 5(a)]. Increasing the x value causes small clusters to merge, and at $x=x_c$ a large enough cluster appears, which provides a completed path for long-range defect diffusion to the surface [Fig. 5(b)]. Further increase of $x>x_c$ results in an expansion of a large cluster [at the expense of the remaining isolated clusters, see Fig. 5(c)], leading to the proportional growth of the diffusion coefficient, shown in Fig. 4.

The latter result can be obtained analytically using Eqs. (2) and (6). At $x-x_c \gg \varepsilon$, Eq. (2) transforms to $C(x) = A \exp[-(x-x_c)/\varepsilon]$, which together with Eq. (6) yields

$$D(x)\cong \frac{L^2}{t_0}\frac{(x-x_c)}{\varepsilon}. \tag{7}$$

Equation (7) provides a linear growth of the diffusion coefficient, $D(x)$, up to a maximum at $x=1$. Note that the $D(x)$

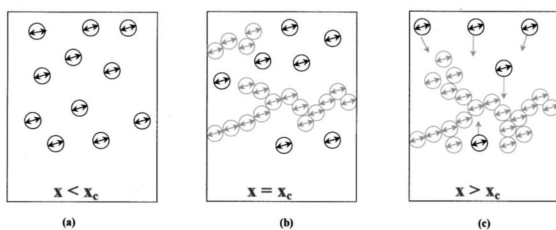

FIG. 5. Schematic illustration of different percolation regimes, depending on the Cd content: (a) $x<x_c$; (b) $x=x_c$; (c) $x>x_c$.

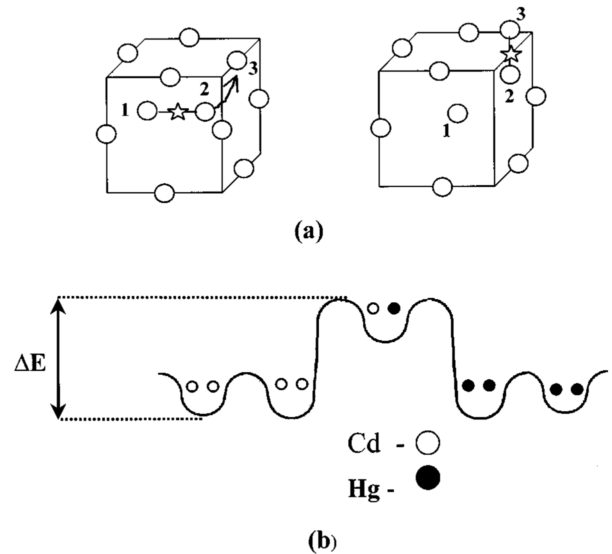

FIG. 6. Schematic presentation of dumbbell interstitials: (a) in real space; (b) energy configuration.

function, calculated using Eqs. (2) and (6), is very similar to the conductance function appearing in the general percolation problem.[27]

It is worthwhile to mention that modification of the percolation properties of crystals under a high implantation dose was previously reported, e.g., for diamond.[30] However, in that case the dosage was enough for partial amorphization of material, so the topology of amorphous regions influenced electrical conductivity of implanted samples. In our situation, an implantation dose is much smaller, and the damaged layer remains a nearly perfect crystal, which is confirmed by dynamical diffraction simulations of measured HRXRD profiles. One can conclude that the damage is mostly related to nonequilibrium point defects, and a percolation problem arises in defect migration during post-implantation lattice recovery.

The microscopic mechanism of point-defect percolation through the fcc structures has been analyzed in detail by Bocquet.[3] In many fcc structures the interstitial positions are too small to accommodate atoms constituting the lattice. So, self-interstitials, if they arise, will push the neighboring atom out of its right position, thus creating a dumbbell-like defect, which already consists of two shifted atoms [see Fig. 6(a)]. During migration the second atom pushes the third one, forming a dumbbell-like defect in the next unit cell, while the first atom returns to the right position. In Ref. 3, migration of dumbbell interstitials is considered for binary alloys (A,B). If only one type of dumbbell interstitial (say B-B) survives, i.e., has minimum formation energy, $E_{BB}<E_{AA}<E_{AB}$ (variant I) or $E_{BB}<E_{AA}=E_{AB}$ (variant II), the calculated percolation threshold to the migration of the B-B dumbbells is $x_{\rm th}=0.278$. The same result, $x_{\rm th}=0.278$, is valid for both species in the case of two surviving defects, A-A and B-B [$E_{BB}=E_{AA}<E_{AB}$ (variant III)]. In this case a long-range migration for A-A (B-B) defects takes place in A (B) clusters, independently. If $E_{AB}=E_{BB}<E_{AA}$ (variant IV) or $E_{AB}<E_{AA}=E_{BB}$ (variant V), the percolation threshold is close to zero.

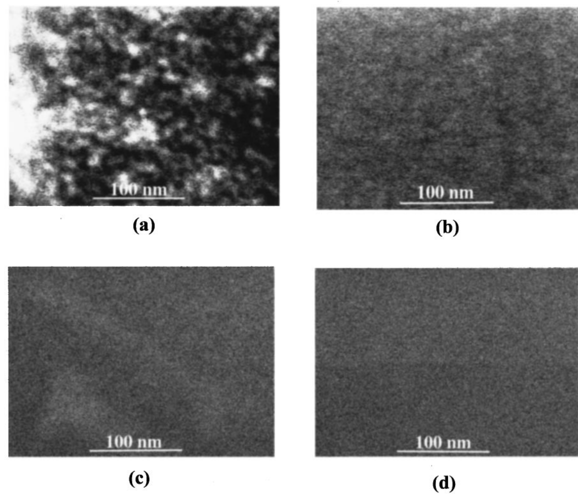

FIG. 7. HRSEM images, demonstrating the ''percolation effect'' in surface recovery in the LPE-grown $Hg_{1-x}Cd_xTe$ layers: (a) virgin sample, $x=0.24$; (b) implanted sample, $x=0.24<x_c$; (c) implanted sample, $x=0.32>x_c$; (d) implanted sample, $x=0.47>x_c$.

This model can be applied to the $Hg_{1-x}Cd_xTe$ ternary alloys, because mixing between fcc sublattices (Te and Hg,Cd) during defect migration at room temperature is negligible. Migration of a certain type of atoms preferably takes place within one sublattice, because the jump to the atomic position belonging to the second sublattice leads to an antisite creation, which increases the system's energy. Percolation problems, in principle, can arise in the (Cd,Hg) sublattice, but not in the Te sublattice, containing only one type of atom.

Proximity of the experimentally found percolation threshold, $x_c=0.265$, to one of the theoretically predicted thresholds, viz., $x_{\mathrm{th}}=0.278$, allowed us to reject variants IV and V of dumbbell configurations. Variants I and II also must be omitted because they do not permit diffusion of A atoms. It implies that a large amount of immovable A-type interstitials will remain in the samples independently of the x value, which contradicts the experimental data. Thus, we have to conclude that the variant III is realized in implanted $Hg_{1-x}Cd_xTe$ layers, i.e., the energies of Cd-Cd and Hg-Hg dumbbells formation are approximately equal and less than the energy of the Cd-Hg dumbbell, as is schematically illustrated in Fig. 6(b). According to energy configuration, only implantation-induced Hg interstitials (besides the Te interstitials) migrate to the sample surface at $x<x_c$, while the Cd species join the company at $x>x_c$.

Two additional experiments were performed in order to support these ideas. The first one is direct imaging of the sample surface in the nm scale using HRSEM. Images, taken under magnification of $\times 400\,000$ from the LPE-grown samples with different x (see Fig. 7), showed remarkable surface modifications after boron implantation, as compared to the virgin samples. In virgin samples, independently of the x value, the contrast variations in a form of light and dark spots in a 10-nm scale were observed [see Fig. 7(a)] and attributed to clusters of point defects.[31] After implantation, the surface of the sample with $x<x_c$, looks much smoother [see Fig. 7(b)] due to partial recovery of defected regions by

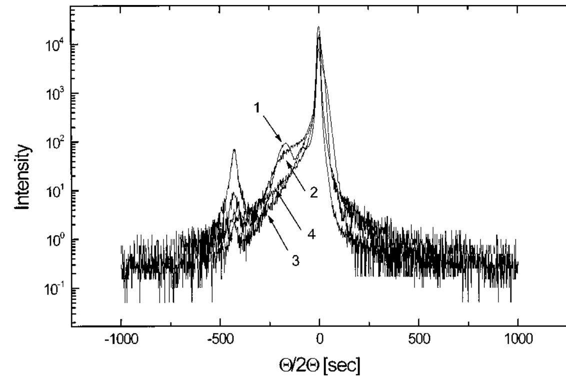

FIG. 8. HRXRD profiles taken from implanted and annealed LPE-grown $Hg_{1-x}Cd_xTe$ layers, demonstrating gradual disappearance of the interstitials peak: as-implanted sample; 2, 3, 4, samples implanted and annealed at 150, 200, and 250 °C, respectively.

a flux of Te and Hg interstitials from the layer interior to the surface. For samples with $x>x_c$, an implantation procedure leads to complete ''healing'' of the surface, as is shown in Figs. 7(c) and 7(d), due to additional flux of the Cd interstitials. Recently, surface recovery in metals after ion implantation has been considered theoretically in terms of dumbbell-interstitials diffusion.[32] Post-implantation defect migration to the sample surface is also taken into account to explain observed modifications of sheet resistance in cold rolled Fe.[33]

The second experiment was carried out with a goal to observe possible changes in ''frozen'' interstitial concentration below x_c in samples subjected to heat treatments at elevated temperatures. Heating serves to overcome a barrier, ΔE, between formation energies of the Cd-Cd and Cd-Hg dumbbells [see Fig. 6(b)], and then to stimulate additional defect migration below x_c. In order to initiate the interstitials transformation, the implanted LPE samples with $x=0.20$ were subjected to the isochronous annealings for 1 h at 150–350 °C. Several HRXRD profiles, taken from implanted and annealed samples, are shown in Fig. 8. Samples subjected to the heat treatments had a rather thin $Hg_{1-x}Cd_xTe$ layer, and hence a third peak (at ≈ -500 arc sec), originating in the CdTe substrate, appears in the profile besides the previously mentioned bulk peak (at 0 angle) and interstitials peak (at ≈ -100–200 arc sec). Certainly, the dynamics of the interstitials peak (which is clearly visible on curve 1 in Fig. 8) is of interest here. In fact, an expected movement of the interstitials peak toward the bulk peak with increasing temperature is evident which indicates an annealing of the remaining interstitials until complete disappearance at 350 °C.

Measured angular positions of the interstitials peak, $\Delta\Theta \sim C$, were again used to follow lattice recovery under heat treatments. It was found that the reduction of the interstitials concentration, C, with increasing temperature, T, is well described in the framework of the Debye relaxation model:

$$C(T,t)-C(\infty)=[C(0)-C(\infty)]e^{-t/\tau} \tag{8}$$

with relaxation time

$$\tau=\tau_0 \exp(\Delta E/kT) \tag{9}$$

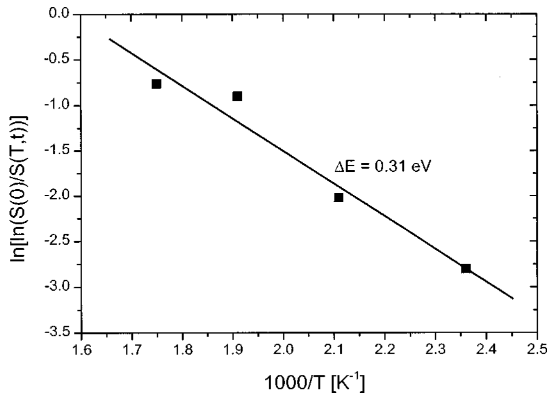

FIG. 9. Arrhenius-like behavior of the interstitials concentration, as a function of annealing temperature T.

exponentially dependent on the energy barrier, ΔE. In Eq. (8), $C(0)$ and $C(\infty)$ stand for the initial ($t=0$) and final ($t=\infty$) concentrations, respectively. If $C(\infty)=0$, Eq. (8) transforms to $S(T,t)=S(0)e^{-t/r}$, which is analogous to Eq. (5), and together with Eq. (9) yields

$$\ln\left[\ln\left(\frac{S(0)}{S(T,t)}\right)\right]=\ln\left(\frac{t}{\tau_0}\right)-\Delta E/kT. \qquad (10)$$

Experimental data plotted in format (10) ($\ln[\ln(S(0)/S(T,t))]$ versus $1/T$) exhibited Arrhenius-like behavior (see Fig. 9), i.e., could be approximated by a straight line, yielding a barrier value of $\Delta E=0.31\pm0.04$ eV.

IV. SUMMARY AND CONCLUSIONS

HRXRD measurements were used to study structural modifications in B-implanted $Hg_{1-x}Cd_xTe$ layers with different Cd contents, x. Due to confinement of most of the damage within a very thin layer, buried at the ion stopping length, we were able to resolve an additional diffraction peak shifted to the left side in the angular scale from the bulk diffraction peak, the latter originating in the undamaged crystal region. Angular position of the additional peak indicated lattice swelling in the damaged area, which was attributed to an excess of interstitials there. Precise measurements of the angular shift mentioned, which is proportional to the interstitials concentration C, were used in order to follow changes in C values under experimental conditions. It was found that interstitials concentration in as-implanted samples exhibits a steplike dependence, as a function of x, with a drastic fall to $C=0$ over a very narrow region, centered at $x_c=0.265$. This behavior indicates a percolation problem (at $x<x_c$) in the Cd transport, involved into the lattice recovery. The obtained threshold value, $x_c=0.265$, was close to the theoretical threshold $x_{th}=0.278$, calculated for dumbbell interstitial defect migration through the fcc lattice.

Due to the percolation problem in the long-range atomic migration (from the bulk to the sample surface) we observed rather different post-implantation surface recovery in samples having $x>x_c$ and $x<x_c$. Supplying additional thermal energy (heat treatments at 150–350 °C), we were able to overcome an energy barrier, ΔE, between the Cd-Cd dumbbells and the Cd-Hg dumbbells, and to stimulate migration of locked defects at $x<x_c$. Thermal activation of Cd-Hg dumbbells leads to the Arrhenius-like kinetics in lattice recovery with $\Delta E=0.31$ eV.

ACKNOWLEDGMENTS

We would like to thank Professor G. Bahir for helpful discussions of the boron activation problem and Dr. A. Sher for supplying MOCVD-grown samples. We are indebted to Dr. A. Berner and Dr. E. Lakin for their help in HRSEM and HRXRD measurements. Contribution of Fermionics Corp., which supplied part of the LPE-grown epilayers for this research, is gratefully acknowledged.

[1] D. Cahen and I. Lubomirski, Chem. Mater. **10**, 2596 (1998).
[2] D. Cahen, O. Melamed, and I. Lubomirski, J. Cryst. Growth **197**, 537 (1998).
[3] J. L. Bocquet, Phys. Rev. B **50**, 16 386 (1994).
[4] *Mercury Cadmium Telluride*, in *Semiconductors and Semimetals*, edited by R. K. Willardson and A. C. Beer (Academic, New York, 1981), Vol. 18.
[5] A. Rogalski and J. Piotrowski, Prog. Quantum Electron. **12**, 205 (1988).
[6] W. E. Tennant, C. A. Cockrum, J. B. Giplin, M. A. Kinch, M. A. Reine, and R. P. Ruth, J. Vac. Sci. Technol. B **10**, 1359 (1992).
[7] L. O. Bubulac and W. E. Tennant, Appl. Phys. Lett. **51**, 355 (1987).
[8] G. L. Destefanis, J. Cryst. Growth **86**, 700 (1988).
[9] R. Kumar, M. B. Dutt, R. Nath, R. Chander, and S. C. Gupta, J. Appl. Phys. **68**, 5564 (1990).
[10] H. F. Schaake, J. Vac. Sci. Technol. A **4**, 2174 (1986).
[11] L. O. Bubulac, J. Cryst. Growth **86**, 723 (1988).
[12] B. L. Williams, H. G. Robinson, and C. R. Helms, Appl. Phys. Lett. **71**, 692 (1997).
[13] B. L. Williams, H. G. Robinson, and C. R. Helms, J. Electron. Mater. **27**, 583 (1998).
[14] H. G. Robinson, B. L. Williams, and C. R. Helms (unpublished).
[15] *Narrow-gap II-VI Compounds for Optoelectronic and Electromagnetic Applications*, in *Electronic Materials Series*, edited by P. Capper (Chapman and Hall, London, 1997), Vol. 3.
[16] L. O. Bubulac, W. E. Tenant, R. A. Riedel, and T. J. Magee, J. Vac. Sci. Technol. **21**, 251 (1982).
[17] T. W. Sigmon, Nucl. Instrum. Methods Phys. Res. B **7/8**, 402 (1985).
[18] G. Bahir, R. Kalish, and Y. Nemirovsky, Appl. Phys. Lett. **41**, 1057 (1982).
[19] J. Baars, A. Hurrle, W. Rothemund, C. R. Ffritzsche, and T. Jakobus, J. Appl. Phys. **53**, 1461 (1982).
[20] B. L. Williams, H. G. Robinson, and C. R. Helms, J. Electron. Mater. **26**, 600 (1997).
[21] N. Mainzer, D. Shilo, E. Zolotoyabko, G. Bahir, and A. Sher, J. Electron. Mater. **26**, 606 (1997).
[22] N. Mainzer, E. Zolotoyabko, A. Berner, E. Lakin, G. Bahir, and A. Sher, J. Cryst. Growth **197**, 542 (1999).

[23] V. Holy, U. Pietsch, and T. Baumbach, *High-Resolution X-Ray Scattering from Thin Films and Multilayers* (Springer-Verlag, Berlin, 1999).
[24] Y. Avrahami and E. Zolotoyabko, Nucl. Instrum. Methods Phys. Res. B **120**, 84 (1996).
[25] M. A. Berding, M. van Schilfgaarde, and A. Sher, Phys. Rev. B **50**, 1519 (1994).
[26] T. Ahilea and E. Zolotoyabko, J. Cryst. Growth **198/199**, 414 (1999).
[27] S. Kirkpatrick, Rev. Mod. Phys. **45**, 574 (1973).
[28] C. Uzan-Saguy, D. Comedi, V. Richter, and R. Kalish, J. Vac. Sci. Technol. A **7**, 2575 (1989).
[29] L. D. Landau and E. M. Lifshitz, *Statistical Physics* (Pergamon, Oxford, 1993).
[30] R. Kalish, T. Bernstein, B. Shapiro, and A. Talmi, Radiat. Eff. **52**, 152 (1980).
[31] N. Mainzer, E. Lakin, G. Bahir, and E. Zolotoyabko, J. Electron. Mater. **28**, 850 (1999).
[32] Yu. N. Osetsky, A. Serra, V. Priego, F. Gao, and D. J. Bacon, in *Diffusion Mechanisms in Crystalline Materials*, edited by Y. Mishin, N. E. B. Cowern, C. R. A. Catlow, D. Farkas, and G. Vogl, Materials Research Society Symposia Proceedings No. 527 (MRS, Pittsburgh, 1998), p. 49.
[33] G. Aggarwal and P. Sen, in *Diffusion Mechanisms in Crystalline Materials* (Ref. 32), p. 111.